Stable boundary treatment for the wave equation on second-order form

Ken Mattsson * Frank Ham† Gianluca Iaccarino‡

June 24, 2008

Abstract

A stable and accurate boundary treatment is derived for the second-order wave equation. The domain is discretized using narrow-diagonal summation by parts operators and the boundary conditions are imposed using a penalty method, leading to fully explicit time integration. This discretization yields a stable and efficient scheme. The analysis is verified by numerical simulations in one-dimension using high-order finite difference discretizations, and in three-dimensions using an unstructured finite volume discretization.

Key words: high-order finite difference methods, unstructured finite volume method, wave equation, numerical stability, second derivatives, boundary conditions, complex geometries

1 Introduction

In many applications, such as general relativity [38, 3], seismology [13, 41], oceanography [31], acoustics [40, 34, 6, 1, 8] and electromagnetics [42, 9], the underlying equations are, or can be, written as systems of second-order hyperbolic partial differential equations. Although these equations can be reduced to first-order symmetric hyperbolic form, this has the disadvantage

*Department of Information Technology, Uppsala University, P O Box 337, S-751 05 Uppsala, Sweden. telephone: +46-18-4717631, telefax: +46-18-523049, E–mail: ken.mattsson@it.uu.se

†Mechanical Engineering - Center for Integrated Turbulence Simulations, Stanford University, US

‡Mechanical Engineering - Flow Physics and Computation, Stanford University, US

of introducing auxiliary variables. (For example, in the harmonic description of general relativity, the principal part of Einstein's equations reduces to 10 curved space wave equations on second order form for the component of the space-time metric, compared to 50 equations when rewritten as a first order system.) The reduction to first-order form is also less attractive from a computational point of view considering the efficiency and accuracy [16, 26]. The reasons for solving the equations on first-order form are most likely related to the maturity of CFD, which has evolved during the last 40 years. I.e., many of the stability issues for first-order hyperbolic problems have already been addressed.

For wave-propagation problems, the computational domain is often large compared to the wavelengths, which means that waves have to travel long distances (or correspondingly long times). It can be shown that high-order accurate time marching methods, as well as high-order spatially accurate schemes (at least third-order) are more efficient [19] for problems on smooth domains. Such schemes, although they might be G-K-S stable [10] (convergence to the true solution as $\Delta x \to 0$), may exhibit a non-physical growth in time [4], for realistic mesh sizes. It is therefore important to devise schemes that do not allow a growth in time that is not called for by the differential equation. Such schemes are called strictly (or time) stable.

In the present study we focus the attention to the second-order formulation of the acoustic wave equation, and the treatment of physical boundaries in particular. A strictly stable high-order accurate finite difference methods (HOFDM) for the wave equation in second order form and discontinuous media was constructed in [26] by combining second-derivative Summation-By-Parts (SBP) operators (constructed in [25]) with the projection method [32, 33] to impose the boundary and the discontinuous interface (jump) conditions. We have in earlier work (regarding first-order systems) [23, 25, 28, 27, 30, 29] advocated the Simultaneous Approximation Term (SAT) method [5] to impose boundary and interface conditions. This technique has recently been used in general relativity (concerning first order systems) [20, 21, 7]. However, the treatment of (for example) Dirichlet boundary conditions and discontinuous media for second-order hyperbolic problems has proven non-trivial using the SAT technique. (This was the main motivation of instead introducing the projection method in [26], since we then failed to find a stable solution using the SAT technique.) In a recent study [24] we have derived a strictly stable treatment of the discontinuous interface (jump) conditions for the second order wave equation in complex 3-D geometries using the SAT technique. In the present study we extend the analysis in [24] to include more general boundary conditions.

In [16, 17, 15, 14] a second-order accurate finite difference method for the

acoustic wave equation on second-order form is constructed, where the discontinuity and complex geometry are handled by embedding the domain into a Cartesian grid, making use of ghost-points and Lagrange interpolation to impose the boundary and interface conditions. It is unclear if the embedded boundary method can be extended to higher-order accuracy. Another good candidate is the discontinuous Galerkin (DG) method (see for example [12]), which combines both unstructured capability and higher-order accuracy. DG have been implemented successfully in 2-D for both the acoustic wave equation [8] and Maxwell's equations [9] on second-order form. However, the efficiency of DG applied to systems of second-order hyperbolic equations on large 3-D applications is an open question.

The purpose of the present study (regarding the acoustic wave equation on second order form) is twofold: 1) to device a strictly stable boundary treatment using the SBP-SAT technique, in particular for the Dirichlet case, and 2) to impose this technique in complex geometries by making use of the discrete Laplacian operator used in CDP[1] (an unstructured finite volume flow solver developed as part of Stanford's DOE-funded ASC Alliance program to perform LES in complex geometries). (This approach is somewhat related to the DG method since they both make use of the penalty technique to handle the boundary conditions.) To the best of our knowledge this is the first time second-order hyperbolic problems in complex 3-D geometries have been addressed using the SBP-SAT technique, with general boundary conditions, including the Dirichlet case.

The motivations for introducing the SAT method instead of the recently developed projection method [26] to impose the boundary conditions are the following: 1) it is easier to implement (although, a detailed study is omitted here), 2) it is not limited to constant speed of sound (see [26]), and 3) it is sometimes much more accurate (as will be shown in Section 4).

The two main reasons for introducing computational tools from CDP are the following: 1) it allows us to handle huge problems in complex geometries, and 2) it makes it easier to isolate and verify the accuracy and stability properties of the Laplacian operator used in CDP. (In spite of it's simplicity the second-order wave equation imposes a stricter stability requirement [26] on the discrete Laplacian operator than when used for parabolic problems such as the Navier-Stokes equations).

In Section 2 we introduce some definitions and discuss the SBP property for the 1-D case, and show how to impose the boundary conditions using SAT. In Section 3 we show how to implement this technique in complex geometries using the unstructured finite volume method. In Section 4 the accuracy and

[1]CDP is named after Charles David Pierce (1969–2002)

stability properties are verified, by performing numerical computations in 1-D and 3-D. A direct comparison between the SAT method and the projection method is done for the 1-D case. In Section 5 we present our conclusions.

In this article, we only consider acoustic waves. The extension to handle for example elastic waves [13, 2, 41] with an analogous approach will be dealt with in a forthcoming paper.

2 The finite difference method

For clarity we will restrict the analysis to 1-D in this section. The extension to 2-D and 3-D (see for example [26, 30, 29]) is straightforward using 1-D SBP finite-difference operators.

We begin with a short description and some definitions (for more details, see [18, 35] and [25]). Let the inner product for real-valued functions $u, v \in L^2[0,1]$ be defined by $(u,v) = \int_0^1 u\,v\,w\,dx$, $w(x) > 0$, and let the corresponding norm be $\|u\|_w^2 = (u,u)$. The domain $(0 \le x \le 1)$ is discretized using $N+1$ equidistant grid points,

$$x_i = i\,h, \quad i = 0, 1..., N, \quad h = \tfrac{1}{N}\ .$$

The approximative solution at grid point x_i is denoted v_i, and the discrete solution vector is $v^T = [v_0, v_1, \cdots, v_N]$. Similarly, we define an inner product for discrete real-valued vector functions $u, v \in \mathbf{R^{N+1}}$ by $(u,v)_H = u^T H\,v$, where $H = H^T > 0$, with the corresponding norm $\|v\|_H^2 = v^T H\,v$. The following vectors will be frequently used:

$$e_0 = [1, 0, ..., 0]^T, \quad e_N = [0, ..., 0, 1]^T\ . \tag{1}$$

2.1 Narrow-diagonal SBP operators

To define narrow-diagonal SBP operators, we present the following definition:

Definition 2.1 *An explicit pth-order accurate finite difference scheme with minimal stencil width of a Cauchy problem, is called a pth-order accurate narrow stencil.*

Remark We say that a scheme is explicit if no linear system of equations need to be solved to compute the difference approximation. Spatial Padé discretizations [22] are often referred to as "compact schemes". The approximation of the derivative is obtained by solving a tri- or penta-diagonal system of linear equations at every time-step. Hence, if written in explicit form, Padé discretizations lead to full-difference stencils, similar to spectral discretizations.

Consider the 1-D wave equation

$$au_{tt} = (bu_x)_x \ , \ x \in [0,\ 1] \tag{2}$$

where $a(x)$, $b(x) > 0$. Multiplying Eq. 2 by u_t and integrating by parts (referred to as "the energy method") lead to

$$\frac{d}{dt}E = 2bu_t u_x|_0^1 \ , \tag{3}$$

where the continuous energy is defined as

$$E = \left(\|u_t\|_a^2 + \|u_x\|_b^2\right) \ . \tag{4}$$

Definition 2.2 *Let $D_2^{(b)} = H^{-1}(-M_b + BS)$ approximate $\partial/\partial\, x\,(\, b\,\partial/\partial\, x)$, where $b(x) > 0$ is a smooth function, using a pth-order accurate narrow stencil. $D_2^{(b)}$ is said to be a pth-order accurate narrow-diagonal second-derivative SBP operator, if H is diagonal and positive definite, M_b is symmetric and positive semi-definite, S approximates the first-derivative operator at the boundaries and $B = diag\,(-b_0, 0 \ldots, 0, b_N)$.*

A second-order accurate narrow-diagonal second-derivative SBP operator $D_2^{(b)}$ was presented in [24]. (High-order accurate narrow-diagonal second-derivative SBP operators for constant coefficients $b(x) = 1$, denoted D_2, were constructed in [25] and later used in [24]). An example of its use is the semi-discretization $Av_{tt} = D_2^{(b)}v$ of (2), where A is the projection of a onto the diagonal. Multiplying by $v_t^T H$ from the left and adding the transpose lead to

$$\frac{d}{dt}E_H = 2(v_t)_0(BSv)_0 + 2(v_t)_N(BSv)_N \ , \tag{5}$$

where the semi-discrete energy is defined as

$$E_H = \left(\|v_t\|_{HA}^2 + v^T M_b v\right) \ . \tag{6}$$

Estimate (5) is a discrete analog of Eq. 3.

Remark The discrete energy (6) mimics Eq. 4 iff: 1) H is diagonal and positive definite, and 2) if M_b is positive semi-definite and the interior stencil is a narrow approximation of $-h\,\partial/\partial\, x\,(\, b\,\partial/\partial\, x)$. The first condition guarantees that the matrix product $H\,A$ is a norm (i.e., symmetric and positive definite). The second condition guarantees that $v^T M_b v \geq 0$ with equality iff v is a constant (such that the quadratic form exactly mimics $\|u_x\|_b$). If M_b is not narrow $v^T M_b v$ is zero also for v equal to the highest frequency mode that can exist on the grid (sometimes referred to as spurious oscillations), which means that stability is not guaranteed.

second-order	fourth-order	sixth-order
1	0.2508560249	0.1878715026

Table 1: α in Eq. 7 for the second-, fourth- and sixth-order accurate narrow-diagonal second-derivative SBP operators.

The following lemma (first introduced in [24]) is central to the present study:

Lemma 2.3 *The dissipative part M_b of a narrow-diagonal second-derivative SBP operator has the following property:*

$$v^T M_b v = h\,\frac{\alpha}{b_0}(BSv)_0^2 + h\,\frac{\alpha}{b_N}(BSv)_N^2 + v^T \tilde{M}_b v\ , \tag{7}$$

where $\tilde{M}_b$ is symmetric and positive semi-definite, and α a positive constant, independent of h.

The poof can be found in [24]. For the special but important case of constant coefficients ($b = 1$) we have derived numerically the values of α for the second-, fourth- and sixth-order accurate finite difference SBP discretizations (listed in [24]) by using the symbolic mathematics software Maple. The results are presented in Table 1.

Remark The boundary closure for a *pth*-order accurate narrow-diagonal SBP operator is of order $p/2$ (see [25]). This means that the boundary closure for $(D_1)^2$ is of order $p/2 - 1$. Hence, for second-order hyperbolic systems the convergence for wide-stencil approximations (i.e., by replacing D_2 with $(D_1)^2$) drops to $(p/2 + 1)th$-order, while the narrow-stencil formulations are $(p/2 + 2)th$-order accurate (see [37] for more information on the accuracy of finite difference approximations).

2.2 The SAT method in 1-D

In this method developed by Carpenter et. al. [4], the boundary conditions are introduced as a penalty term. When the energy method is applied, a discrete analog to the continuous energy is obtained. However, the treatment of Dirichlet boundary conditions introduce some difficulties for second order hyperbolic problems, which is the main focus of the present study.

Consider Eq. 2. General boundary conditions are given by

$$\begin{array}{ll} L_0 u = \beta_1 u - \beta_2 b u_x + \beta_3 u_t = g_0(t), & x = 0 \\ L_1 u = \beta_1 u + \beta_2 b u_x + \beta_3 u_t = g_1(t), & x = 1 \end{array}\ . \tag{8}$$

Note that (8) includes the special case of Dirichlet boundary conditions (and radiation boundary conditions. See for example [39] and [11]).

2.2.1 Mixed boundary conditions

The case where $\beta_2 \neq 0$ includes the important case of Neumann boundary conditions ($\beta_1 = 0,\ \beta_2 = 1,\ \beta_3 = 0$). To simplify the analysis we assume that the boundary data is homogeneous. (The analysis holds for inhomogeneous data, but introduces unnecessary notation.) The energy method applied to (2) with the boundary conditions (8) leads to

$$\frac{d}{dt}\left(\|u_t\|_a^2 + \|u_x\|_b^2 + \frac{\beta_1}{\beta_2}u_0^2 + \frac{\beta_1}{\beta_2}u_1^2\right) = -\frac{\beta_3}{\beta_2}(u_t^2)_0 - \frac{\beta_3}{\beta_2}(u_t^2)_1 \ . \tag{9}$$

The problem have an energy estimate if

$$\frac{\beta_1}{\beta_2} \geq 0 \ , \ \frac{\beta_3}{\beta_2} \geq 0 \ . \tag{10}$$

A semi-dicretization of (2) using a narrow-diagonal SBP operator, and the SAT method to impose the boundary conditions (8), can be written

$$HAv_{tt} = (-M_b + BS)v + \tau e_0\left(L_0^T v - g_0\right) + \tau e_N\left(L_1^T v - g_1\right) \ . \tag{11}$$

The discrete versions of (8) are given by

$$\begin{array}{l} L_0^T v = \beta_1 v_0 + \beta_2 (BSv)_0 + \beta_3 (v_t)_0 = g_0 \\ L_1^T v = \beta_1 v_N + \beta_2 (BSv)_N + \beta_3 (v_t)_N = g_1 \ . \end{array} \tag{12}$$

Lemma 2.4 *The scheme (11) with homogenous data is stable if $D_2^{(b)}$ is a narrow-diagonal second-derivative SBP operator, $\tau = -1/\beta_2$ and (10) hold.*

Proof Let $g_0,\ g_1 = 0$. Multiplying (11) by v_t^T from the left and adding the transpose lead to

$$\begin{aligned} v_t^T H\, Av_{tt} + v_{tt}^T A\, Hv_t = &- v_t^T M_b v - v^T M_b^T v_t + 2(v_t)_0 (BSv)_0 + 2(v_t)_N (BSv)_N \\ &+ 2\tau (v_t)_0 (\beta_1 v_1 + \beta_2 (BSv)_0 + \beta_3 (v_t)_0) \\ &+ 2\tau (v_t)_N (\beta_1 v_N + \beta_2 (BSv)_N + \beta_3 (v_t)_N) \end{aligned} \ .$$

If $D_2^{(b)}$ is a narrow-diagonal second-derivative SBP operator, we obtain

$$\begin{aligned} \frac{d}{dt}\left(\|v_t\|_{H\,A}^2 + v^T M_b v - \tau\beta_1 v_0^2 - \tau\beta_1 v_N^2\right) = &+ \tau\beta_3 (v_t)_0^2 + \tau\beta_3 (v_t)_N^2 \\ &+ 2(1+\tau\beta_2)(v_t)_0 (BSv)_0 + 2(1+\tau\beta_2)(v_t)_N (BSv)_N \end{aligned} \ .$$

If $\tau = -1/\beta_2$ we obtain an energy estimate completely analogous to (9). If (10) holds we have a non-growing energy. $\square$

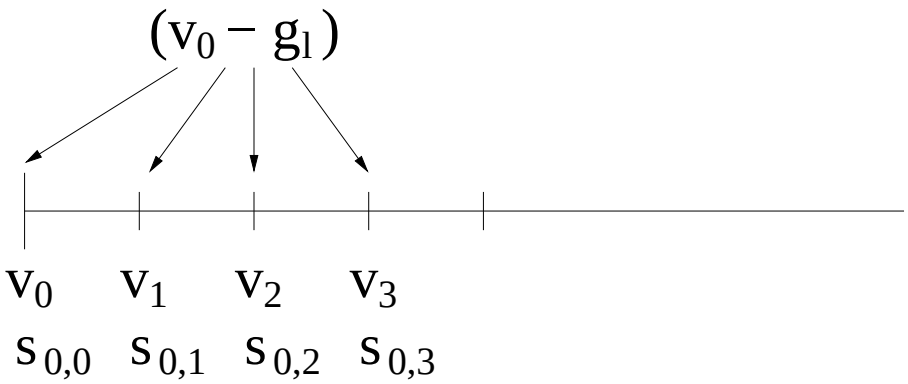

Figure 1: An illustration how the $(BS)^T$ penalty for weakly imposed Dirichlet conditions will influence the four points closest to the boundary, using the fourth-order accurate operator. Here $s_{0,3} = \frac{1}{3}$ is the fourth parameter in S.

2.2.2 Dirichlet boundary conditions

With Dirichlet boundary conditions ($\beta_1 = 1,\ \beta_2 = 0,\ \beta_3 = 0$) and homogenous data, the energy method applied to (2) leads to

$$\frac{d}{dt}\left(\|u_t\|_a^2 + \|u_x\|_b^2\right) = 0\ . \tag{13}$$

A semi-dicretization of (2) using a narrow-diagonal SBP operator, and the SAT method to impose the Dirichlet boundary conditions (8), can be written

$$\begin{aligned} HAv_{tt} = (-M_b + BS)v \quad & +\epsilon(BS)^T e_0\,(v_0 - g_0) + \sigma b_0 e_0\,(v_0 - g_0) \\ & +\epsilon(BS)^T e_N\,(v_N - g_1) + \sigma b_N e_N\,(v_N - g_1)\ . \end{aligned} \tag{14}$$

Remark The two penalties in (14) that are multiplied by $(BS)^T$ will impose the Dirichlet boundary conditions weakly at all points used in the reconstruction of the boundary derivatives, i.e., $(BSv)_{0,\,N}$. The left boundary derivative approximation of the fourth-order accurate operator (see for example [24]) requires 4 points in the reconstruction. This means that the four points closest to the boundaries, see Figure 1, will be penalized, with the weights given by the coefficients in S.

The first main result of this paper is stated in the following Lemma:

Lemma 2.5 *The scheme (14) with homogenous data is stable if $D_2^{(b)}$ is a narrow-diagonal second-derivative SBP operator, $\sigma \leq -\frac{1}{\alpha h}$ and $\epsilon = 1$ hold.*

Proof Let $g_0,\, g_1 = 0$. Multiplying (14) by v_t^T from the left and adding the transpose lead to

$$\begin{aligned} v_t^T H\, A v_{tt} + v_{tt}^T A\, H v_t = &- v_t^T M_b v - v^T M_b^T v_t + 2(v_t)_0 (BSv)_0 + 2(v_t)_N (BSv)_N \\ &+ 2\epsilon (BSv_t)_0 v_0 + 2\sigma b_0 (v_t)_0 v_0 \\ &+ 2\epsilon (BSv_t)_N v_N + 2\sigma b_N (v_t)_N v_N \end{aligned} \quad .$$

Two necessary stability requirements are that $\epsilon = 1$ and that $M_b = M_b^T$ is positive semi-definite. By using Lemma 2.3 and the fact that $D_2^{(b)}$ is a narrow-diagonal second-derivative SBP operator we obtain

$$\frac{d}{dt}\left(\|v_t\|_{H\,A}^2 + v^T \tilde{M} v + w_0^T R_0 w_0 + w_N^T R_N w_N \right) = 0 \;,$$

where $w_{0,\,N}^T = [v_{0,\,N} \;,\; (BSv)_{0,\,N}]$ and

$$R_0 = \begin{bmatrix} -\sigma b_0 & -1 \\ -1 & \frac{\alpha\, h}{b_0} \end{bmatrix}, \quad R_N = \begin{bmatrix} -\sigma b_N & -1 \\ -1 & \frac{\alpha\, h}{b_N} \end{bmatrix} \;.$$

Stability follows if $\sigma \leq -\frac{1}{\alpha\, h}$ holds. $\square$

We introduce the penalty-strength parameter γ through

$$\sigma = -\gamma \frac{1}{\alpha\, h} \;.$$

Hence a value of $\gamma < 1$, according to Lemma 2.5, will not result in an energy estimate and might lead to an unstable scheme. A higher value of γ leads to a more tight imposition of the Dirichlet boundary condition. This can potentially lead to a more accurate solution, but will also introduce stiffness. This is verified numerically in Section 4.

3 The finite volume method

In this section we will extend the present 1-D analysis to 3-D complex geometries utilizing the discrete Laplacian finite volume operator used to develop the internal discretization and boundary conditions in CDP. The operator is developed for a node-based discretization on general polyhedral meshes, where both grid coordinates and the unknowns are collocated at nodes. The discretization of the Laplacian operator is particularly challenging for unstructured finite volume methods because it is difficult (see [36]) to simultaneously achieve accuracy and stability on general unstructured grids. Details

of the discretization is presented in [24]. We begin with a short description and some definitions. Consider the 3-D wave equation

$$a u_{tt} = b\,\Delta u \tag{15}$$

where b, $a(x, y, z) > 0$. To simplify notation in this section we assume that b is constant (compare with Eq. 2 in 1-D), although CDP can handle variable coefficients.

To define the narrow-diagonal Laplacian operator (compare with Definition 2.2 in the 1-D case.), we present the following two definitions:

Definition 3.1 *Let* $S = \sum_{i \in F_b'} S_{i,b}$, *where* F_b' *is the set of all boundary sub-faces.* $S_{i,b}$ *is an outward sub-face normal derivative operator associated with each of the boundary nodes. We say that* S *approximates the outward normal derivative operator at the boundary.*

Definition 3.2 *Let* $D_L = V^{-1}(-L+S)$ *approximate the Laplacian operator.* D_L *is said to be a narrow-diagonal Laplacian SBP operator, if* V *is diagonal and positive definite,* L *is narrow, symmetric and positive semi-definite, and* S *as defined in Definition 3.1.*

A semi-discretization of (15), using a narrow-diagonal Laplacian SBP operator, will have the following matrix form:

$$V\,A v_{tt} = b(-L + S)v\ . \tag{16}$$

In Section 4 we will use this operator to simulate wave-propagation in complex 3-D geometry.

The following lemma (first presented in [24]) is central to the present study:

Lemma 3.3 *The dissipative part* L *of a narrow-diagonal Laplacian SBP operator has the following property:*

$$v^T L v = \alpha \sum_{i \in F_b'} \frac{V_{i,b}}{A_{i,b}} (S_{i,b} v)^2 + v^T \tilde{L} v\ , \tag{17}$$

where F_b' *is the set of all boundary sub-faces and* $S_{i,b}$ *as in Definition 3.1.* $A_{i,b}$ *is an area magnitude, and* $V_{i,b}$ *a nodal volume associated with each of the boundary nodes.* $\tilde{L}$ *is symmetric and positive semi-definite and* α *a positive constant.*

We omit the proof, since it is similar to the proof of Lemma 2.3. Unlike the uniform structured 1-D case, it is more complicated to analytically derive a single sharp value for α, that is applicable to all unstructured grids. A numerical eigenvalue analysis indicate that $\alpha \simeq 0.8$ for the problems computed in this article (compare with the second-order case in 1-D Table 1).

Consider Eq. 15. General boundary conditions are given by (compare with (8) in 1-D)

$$Lu = \beta_1 u + \beta_2 b \nabla \cdot \mathbf{n} u + \beta_3 u_t = g(t) \quad \mathbf{x} \in \partial\Omega \quad . \tag{18}$$

The domain Ω is in $\mathbf{R^3}$ and the boundary is $\partial\Omega$. ∇ is the gradient operator and $\mathbf{n}$ is the outward pointing normal.

3.1 Mixed boundary conditions in 3-D

A semi-discretization of (15) using a narrow-diagonal Laplacian SBP operator, and the SAT method to impose the boundary conditions (18), can be written as

$$VAv_{tt} = b(-L+S)v + \tau B_{i,b}^{(1)}(L^T v - g) \ , \tag{19}$$

where $B_{i,b}$ picks out the boundary nodes (compare with $e_{0,N}$ in (1)). The discrete version of (18) is given by

$$L^T v = \beta_1 v + \beta_2 S v + \beta_3 v_t = g \ . \tag{20}$$

Lemma 3.4 *The scheme (19) with homogenous data is stable if $D_L = V^{-1}(-L+S)$ is a narrow-diagonal Laplacian SBP operator, $\tau = -1/\beta_2$ and (10) hold.*

We omit the proof, since it is similar to the proof of Lemma 2.4.

3.2 Dirichlet boundary conditions in 3-D

A semi-discretization of (15) using a narrow-diagonal Laplacian SBP operator, and the SAT method to impose the Dirichlet boundary conditions ($\beta_1 = 1,\ \beta_2 = 0,\ \beta_3 = 0$ in (18)), can be written as

$$VAv_{tt} = b(-L+S) + \epsilon S^T B_{i,b}(v-g) + \sigma_{i,b} B_{i,b}(v-g) \ . \tag{21}$$

The second main result of this paper is stated in the following Lemma:

Lemma 3.5 *The scheme (21) with homogenous data is stable if $D_L = V^{-1}(-L+S)$ is a narrow-diagonal Laplacian SBP operator, $\sigma_{i,b} \leq -\frac{A_{i,b}}{V_{i,b}}\frac{1}{\alpha}$ and $\epsilon = 1$ hold.*

We omit the proof, since it is similar to the proof of Lemma 2.5. (Note that $\sigma_{i,b}$ varies along the boundary depending on $A_{i,b}$ and $V_{i,b}$.)

4 Computations

To verify the accuracy of (11), (14), (19) and (21), we chose an analytic (standing wave) solution

$$u = cos(m\,\pi\,b\,t)\,cos(m\,\pi\,a\,x),\ m \in \mathbf{Z}. \tag{22}$$

The convergence rate is calculated as

$$q = \log_{10}\left(\frac{\|u - v^{(N_1)}\|_h}{\|u - v^{(N_2)}\|_h}\right) / \log_{10}\left(\frac{N_1}{N_2}\right)^{1/d}\ , \tag{23}$$

where d is the dimension ($d = 1$ in the 1-D case), u is the analytic solution, and $v^{(N_1)}$ the corresponding numerical solution with N_1 unknowns. $\|u - v^{(N_1)}\|_h$ is the discrete l_2 norm of the error.

Eq. 11, 14, 19 and 21 (with $\sigma = 0$) and homogeneous data can formally be written as an ODE system

$$v_{tt} = Qv\ , \tag{24}$$

where v^T is the discrete solution vector. In Sections 2 and 3 we have shown that the matrix Q have non-positive and real eigenvalues (a necessary stability condition) by utilizing the energy method. A compact (only two time-levels have to be stored) and explicit high-order accurate time-discretization is used (see [26]) for the time advancement. For a Cartesian grid it can be shown [26] that the time-step restriction (for stability) is inversely proportional to the square root of the spectral radius of Q.

4.1 High-order finite difference method in 1-D

The spectral radius of $\tilde{Q} = h^2\,Q$ for the semi-discrete problem Eq. 14 as a function of the penalty strength γ is presented in Table 3. We compare the second-, fourth- and the sixth-order accurate cases, and include the corresponding results using the projection method (see [26] for details). The stiffness increases with a larger γ. (For completeness we also compute the spectral radius of Eq. 11, using Neumann boundary conditions, presented in Table 2.) If the conditions in Lemma 2.5 are not fulfilled we might introduce positive and/or imaginary eigenvalues, resulting in an unstable scheme. This is verified numerically by computing the eigenvalues to $\tilde{Q}$. The results for the sixth order discretization of (14) with $a = b = 1$ are shown in Figure 2.

The convergence results for the Dirichlet case (14) are shown in Tables 4–6 showing the improved accuracy with increased penalty strength γ. A

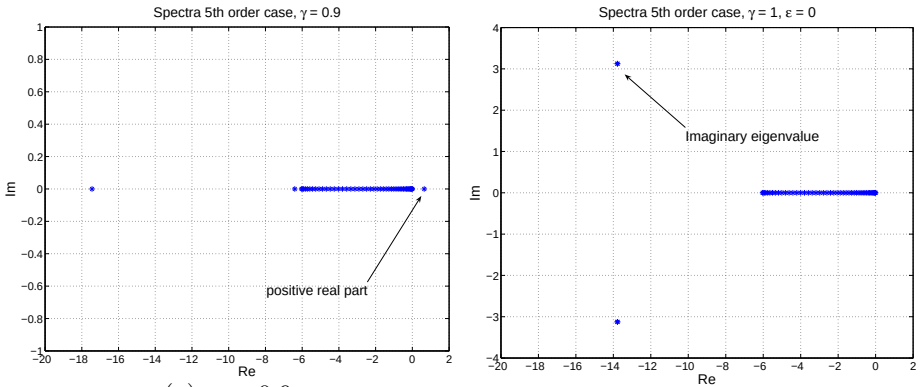

(a) $\gamma = 0.9$ (b) $\gamma = 1$, $\epsilon = 0$

Figure 2: The eigenvalues to $\tilde{Q}$ for the sixth order case and different choice of unstable penalty parameters. (a) with $\gamma = 0.9$ and (b) with $\gamma = 1$, $\epsilon = 0$.

direct comparison with the projection method [26] is also presented. The simulation is run to $t = 1.1$ (and we use $a = b = 1$ and $m = 8$) with a time step small enough to make the time discretization error negligible (compared to the spatial discretization error). The SAT method is slightly less accurate (for $\gamma > 1$) than the projection method. The sixth-order case should in theory only lead to fifth-order convergence (see [37] for more information on the accuracy of finite difference approximations), but yields a result closer to seventh-order (see Table 6). (This is a remarkable result that needs further study since it contradicts the convergence analysis in [37].)

The convergence results of (11) using Neumann boundary conditions are shown in Tables 7–9, including a comparison with the projection method [26]. Again the simulation is run to $t = 1.1$ using the same small time-step. The SAT method is now much more accurate than the projection method, and leads to a higher convergence rate. The spectral radius of $\tilde{Q}$ are now almost identical (except for the sixth-order case), see Table 2.

To summarize this study. The SAT method is clearly superior when using Neumann boundary conditions (similar to the results in [24] when focusing on discontinuous jump conditions). When using Dirichlet boundary conditions for this particular problem, the projection is slightly more efficient. However, the projection method is restricted to piecewise constant variables (see [26]). The SAT method does not have this limitation.

Order	SAT	$Proj$
second	4.00	4.28
fourth	5.33	5.33
sixth	14.18	8.83

Table 2: The spectral radius of h^2Q for Eq. 11, sixth order case. Also comparing to the projection method.

Order	$\gamma = 1$	$\gamma = 1.2$	$\gamma = 5$	$Proj$
second	4.10	4.28	21.14	4.00
fourth	7.70	9.00	49.05	5.33
sixth	17.89	19.05	75.65	13.94

Table 3: The spectral radius of h^2Q for Eq. 14 using different strength of penalty parameter γ, sixth order case. Also comparing to the projection method.

N	$\gamma = 1$	$q(1)$	$\gamma = 1.2$	$q(1.2)$	$\gamma = 5$	$q(5)$	$Proj$	$q(P)$
51	-1.05	0.00	-1.13	0.00	-1.10	0.00	-1.10	0.00
101	-1.66	2.02	-1.68	1.81	-1.68	1.91	-1.68	1.92
201	-2.27	2.02	-2.28	1.98	-2.28	1.98	-2.28	1.98

Table 4: $log(l_2 - error)$ and convergence for Eq. 14, second-order case and different values of γ. Also comparing to the projection method.

N	$\gamma = 1$	$q(1)$	$\gamma = 1.2$	$q(1.2)$	$\gamma = 5$	$q(5)$	$Proj$	$q(P)$
51	-1.38	0.00	-2.04	0.00	-2.26	0.00	-2.26	0.00
101	-2.07	2.29	-3.41	4.54	-3.55	4.29	-3.55	4.28
201	-2.81	2.45	-4.67	4.19	-4.80	4.14	-4.80	4.14

Table 5: $log(l_2 - error)$ and convergence for Eq. 14, fourth-order case and different values of γ. Also comparing to the projection method.

N	$\gamma = 1$	$q(1)$	$\gamma = 1.2$	$q(1.2)$	$\gamma = 5$	$q(5)$	$Proj$	$q(P)$
51	-1.59	0.00	-2.11	0.00	-2.94	0.00	-3.01	0.00
101	-2.85	4.21	-4.12	6.66	-4.84	6.32	-4.92	6.37
201	-4.19	4.43	-6.16	6.78	-6.89	6.81	-7.03	6.99

Table 6: $log(l_2 - error)$ and convergence for Eq. 14, sixth-order case and different values of γ. Also comparing to the projection method.

N	SAT	$q(S)$	$Proj$	$q(P)$
51	-0.84	0.00	-0.03	0.00
101	-1.50	2.18	-0.91	2.92
201	-2.12	2.05	-1.77	2.87

Table 7: $log(l_2 - error)$ and convergence for Eq. 11, second-order case. Also comparing to the projection method.

N	SAT	$q(S)$	$Proj$	$q(P)$
51	-2.33	0.00	-0.11	0.00
101	-3.52	3.93	-0.94	2.76
201	-4.75	4.10	-1.83	2.94

Table 8: $log(l_2 - error)$ and convergence for Eq. 11, fourth-order case. Also comparing to the projection method.

N	SAT	$q(S)$	$Proj$	$q(P)$
51	-2.88	0.00	-0.56	0.00
101	-5.06	7.23	-2.01	4.83
201	-7.01	6.47	-3.50	4.95

Table 9: $log(l_2 - error)$ and convergence for Eq. 11, sixth-order case. Also comparing to the projection method.

N	$log(l_2)$	q
46,680	-1.46	-
373,440	-2.08	2.056
2,987,520	-2.69	2.028
23,900,160	-3.30	2.003

Table 10: Unstructured grid refinement study: reduction in l_2 error with grid refinement, imposing Eq. 22 as boundary and initial data. N is the total number of tetrahedra in the grid. Errors are reported at the peak in l_2 error at $t = 0.54$..

4.2 Finite volume method in 3-D

The present method has been implemented for unstructured tetrahedral grids, using the node-based SBP finite-volume discretization (presented in Section 3). A triply-periodic tetrahedral mesh was generated around a $2 \times 2 \times 2$ array of three cube compounds. Inspiration for this choice of geometry comes from M. C. Escher's Waterfall (see Figure 4). Our cubes have a characteristic dimension of 0.2, and have center-to-center spacing of 0.5 in a $1 \times 1 \times 1$ box. The simulation of the wave equation in the surrounding volume requires an unstructured mesh to capture the complex polyhedral boundaries, although at any resolution the boundaries are precisely represented because all surfaces are planar. This allows us to generate a series of fine grids starting from a coarse grid by recursively applying a tetrahedral-splitting algorithm. Some details of the mesh are provided in Figure 5.

In the first test we verify the accuracy of Eq. 21. We chose the analytic 1-D solution given by Eq. 22, and compute the solution on the geometry defined by the cube compounds. (As for the 1-D case we use $a = b = 1$ and $m = 8$.) A grid convergence study is shown in Table 10. The exact solution is imposed as initial- and boundary-data (i.e., also at the boundaries of the complex 3-D cubes). The grid sizes range from 46,680 tetrahedra up to 23,900,160 tetrahedra on the finest grid. To illustrate the importance of choosing γ large enough, we show in Figure 3 the evolution of l_2 error over time. The time term is discretized using the standard second-order discretization. The numerical simulations verify that $\gamma \approx 1$ for this particular problem. Further increases in γ improves the accuracy of the solution, although there is also an increase in stiffness and a reduction of the computational time step was required for $\gamma > 5$.

In the final test we compute the 3-D propagation of a Gaussian pulse in the volume surrounding the $2 \times 2 \times 2$ array of 3-cube compounds. The simulations were initiated with a Gaussian (3-D) profile given by $exp(-((x -$

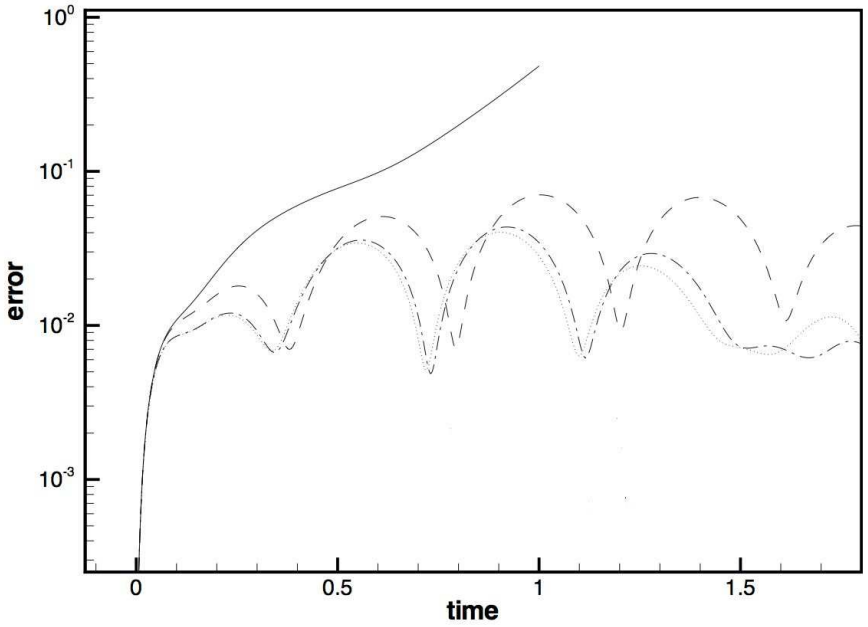

Figure 3: Time history of l_2 error for 4 different values of penalty strength γ for the standing wave simulation with coarsest triply-periodic unstructured grid. *solidline*: $\gamma = 0.99$; *dashedline*: $\gamma = 1$; *dashed − dottedline*: $\gamma = 1.2$; *dottedline*: $\gamma = 5$

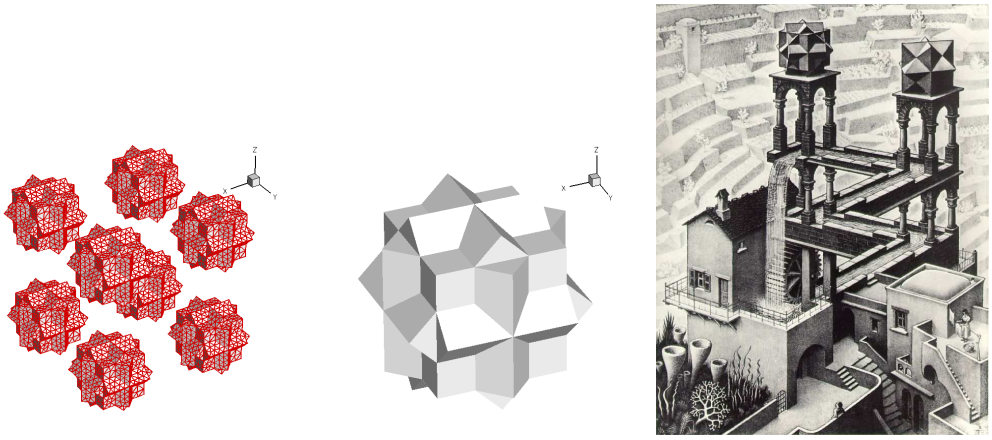

Figure 4: Geometrical details and inspiration for the three cube compounds.

$x_c)^2 + (y - y_c)^2 + (z - z_c)^2)/0.03^2)$ (centered at (x_c, y_c, z_c)) in the plane of four of the polyhedra and offset slightly along the diagonal to break the four-fold symmetry. Hence, the solution should not be entirely symmetric. We impose the homogeneous Neumann- and Dirichlet-boundary conditions at the boundaries of the complex 3-D cubes. The simulations presented in Figure 6 were run on the finest grid (see Table 10) produced by 3 applications of recursive tetrahedral refinement to this coarse grid. The time step is $\Delta t = 0.00025$. Results are plotted on a plane passing through the center of four of the polyhedra for three times, $t = 0.25$, $t = 0.5$, and $t = 0.75$. The location of the center of the initial pulse is in this plane and displaced slightly toward the upper right, producing the observed diagonal asymmetry.

Remark These last simulations were done primarily to show that the present SBP-SAT technique can be utilized for large scale simulations using computational tools from the production code CDP. A grid convergence study for these problems were not performed, since it would be very costly to derive reference solutions. An assessment of the number of unknowns needed to resolve the wave-propagation was not done. Hence, the purpose were not to resolve any particular physics-application. It was shown as an illustration of the methods capability and stability properties.

5 Conclusions and future work

We have proven that narrow-stencil approximations of the second-order acoustic wave equation with general boundary conditions are time-stable, when

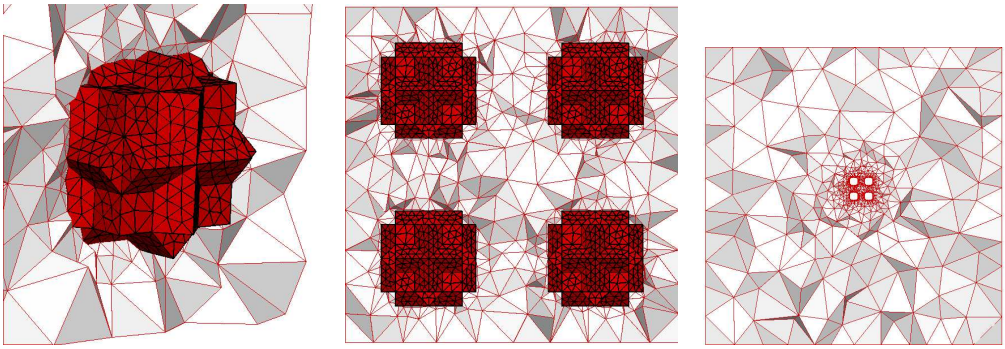

Figure 5: Plane cut through coarse grid, different views (zoom).

combining narrow-diagonal SBP operators and the SAT penalty technique to impose the boundary conditions. The accuracy and stability of the present method have been verified by numerical simulations in 1-D using high-order finite difference discretizations and in 3-D using the unstructured finite volume discretization utilized by the production code CDP. A direct comparison with the projection method was done in 1-D, with the conclusion that the newly constructed SAT method is much more efficient, except for Dirichlet boundary conditions.

Future work will include the application of the present SBP-SAT technique to systems of second-order hyperbolic equations such as the elastic wave equations, Einstein's equations and Maxwell's equations. To further increase the efficiency of the method we will propose a hybrid discretization, by combining (using the SAT technique) the high-order accurate SBP discretizations and the unstructured SBP discretization discussed in the present study.

References

[1] A. Bamberger, R. Glowinski, and Q.H Tran. A domain decomposition method for the acoustic wave equation with discontinuous coefficients and grid change. *SIAM J. Num. Anal.*, 34(2):603–639, 1997.

[2] A. Bayliss, K. E. Jordan, B. J. Lemesurier, and E. Turkel. A fourth order accurate finite difference scheme for the computation of elastic waves. *Bull. Seismol. Soc. Amer.*, 76(4):1115–1132, 1986.

[3] G. Calabrese. Finite differencing second order systems describing black holes. *Physical Review D*, 71:027501, 2005.

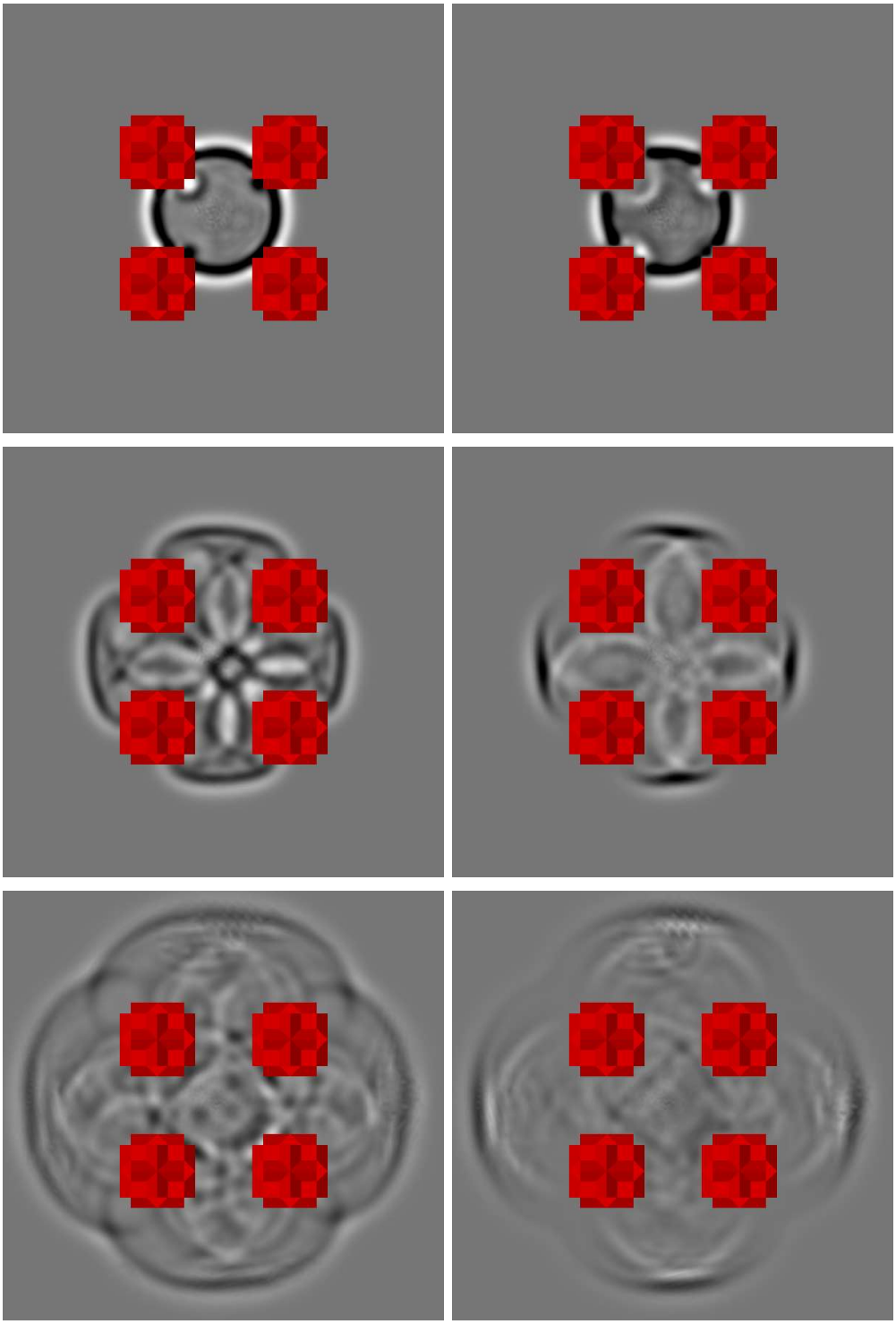

Figure 6: Propagation of a 3D Gaussian pulse comparing Neumann (left column) and Dirichlet (right column) boundary conditions (for three times, $t = 0.25$, $t = 0.5$, and $t = 0.75$) on the $2 \times 2 \times 2$ array of 3-cube compounds.

[4] M. H. Carpenter, D. Gottlieb, and S. Abarbanel. Time-stable boundary conditions for finite-difference schemes solving hyperbolic systems: Methodology and application to high-order compact schemes. *J. Comput. Phys.*, 111(2), 1994.

[5] M. H. Carpenter, D. Gottlieb, and S. Abarbanel. Time-stable boundary conditions for finite-difference schemes solving hyperbolic systems: Methodology and application to high-order compact schemes. *J. Comput. Phys.*, 111(2), 1994.

[6] G. Cohen and P. Joly. Construction and analysis of fourth-order finite difference schemes for the acoustic wave equation in nonhomogeneous media. *SIAM J. Num. Anal.*, 33(4):1266–1302, 1996.

[7] Peter Diener, Ernst Nils Dorband, Erik Schnetter, and Manuel Tiglio. Optimized high-order derivative and dissipation operators satisfying summation by parts, and applications in three-dimensional multi-block evolutions. *J. Sci. Comput.*, 32(1):109–145, 2007.

[8] M. Grote, A. Schneebeli, and D. Schötzau. Discontinuous Galerkin finite element method for the wave equation. *SIAM J. Num. Analysis*, 44:2408–2431, 2006.

[9] M. Grote, A. Schneebeli, and D. Schötzau. Interior penalty discontinuous galerkin method for maxwell's equations: Energy norm error estimates. *Journal of Computational and Applied Mathematics*, 204:375–386, 2007.

[10] B. Gustafsson, H. O. Kreiss, and A. Sundström. Stability theory of difference approximations for mixed initial boundary value problems. *Math. Comp.*, 26(119), 1972.

[11] T. Hagstrom. Radiation boundary conditions for the numerical simulation of waves. *Acta Numerica*, pages 47–106, 1999.

[12] J. S. Hesthaven and T. Warburton. *Nodal Discontinuous Galerkin Methods: Algorithms, Analysis, and Applications*. Springer Verlag, New York, 2008.

[13] K. R. Kelly, R. W. Ward, S. Treitel, and R. M. Alford. Synthetic seismograms: A finite difference approach. *Geophysics*, 41:2–27, 1976.

[14] H.-O. Kreiss and N.A. Petersson. An embedded boundary method for the wave equation with discontinuous coefficients. *SIAM J. Sci. Comput.*, 28:2054–2074, 2006.

[15] H.-O. Kreiss and N.A. Petersson. A second order accurate embedded boundary method for the wave equation with dirichlet data. *SIAM J. Sci. Comput.*, 27:1141–1167, 2006.

[16] H.-O. Kreiss, N.A. Petersson, and J. Yström. Difference approximations for the second order wave equation. *SIAM J. Num. Anal.*, 40:1940–1967, 2002.

[17] H.-O. Kreiss, N.A. Petersson, and J. Yström. Difference approximations of the Neumann problem for the second order wave equation. *SIAM J. Num. Anal.*, 42:1292–1323, 2004.

[18] H.-O. Kreiss and G. Scherer. Finite element and finite difference methods for hyperbolic partial differential equations. *Mathematical Aspects of Finite Elements in Partial Differential Equations., Academic Press, Inc.*, 1974.

[19] Heinz-Otto Kreiss and Joseph Oliger. Comparison of accurate methods for the integration of hyperbolic equations. *Tellus XXIV*, 3, 1972.

[20] L. Lehner, D. Neilsen, O. Reula, and M. Tiglio. The discrete energy method in numerical relativity: towards long-term stability. *Classical Quantum Gravity*, 21:5819–5848, 2004.

[21] L. Lehner, O. Reula, and M. Tiglio. Multi-block simulations in general relativity: high-order discretizations, numerical stability and applications. *Classical Quantum Gravity*, 22:5283–5321, 2005.

[22] S. K. Lele. Compact finite difference schemes with spectral-like resolution. *J. Comput. Phys.*, 103:16–42, 1992.

[23] K. Mattsson. Boundary procedures for summation-by-parts operators. *Journal of Scientific Computing*, 18:133–153, 2003.

[24] K. Mattsson, F. Ham, and G. Iaccarino. Stable and accurate wave propagation in discontinuous media. *J. Comput. Phys.*, To appear, 2008.

[25] K. Mattsson and J. Nordström. Summation by parts operators for finite difference approximations of second derivatives. *J. Comput. Phys.*, 199(2):503–540, 2004.

[26] K. Mattsson and J. Nordström. High order finite difference methods for wave propagation in discontinuous media. *J. Comput. Phys.*, 220:249–269, 2006.

[27] K. Mattsson, M. Svärd, M.H. Carpenter, and J. Nordström. High-order accurate computations for unsteady aerodynamics. *Computers & Fluids*, 36:636–649, 2006.

[28] K. Mattsson, M. Svärd, and J. Nordström. Stable and Accurate Artificial Dissipation. *Journal of Scientific Computing*, 21(1):57–79, August 2004.

[29] K. Mattsson, M. Svärd, and M. Shoeybi. Stable and accurate schemes for the compressible navier-stokes equations. *J. Comput. Phys.*, 227(4):2293–2316, 2008.

[30] J. Nordström, K. Mattsson, and R.C. Swanson. Boundary conditions for a divergence free velocity-pressure formulation of the incompressible navier-stokes equations. *J. Comput. Phys.*, 225:874–890, 2007.

[31] J. Nycander. Tidal generation of internal waves from a periodic array of steep ridges. *J. Fluid Mech.*, 567:415–432, 2006.

[32] P. Olsson. Summation by parts, projections, and stability I. *Math. Comp.*, 64:1035, 1995.

[33] P. Olsson. Summation by parts, projections, and stability II. *Math. Comp.*, 64:1473, 1995.

[34] G.R. Shubin and J.B. Bell. A modified equation approach to constructing fourth order methods for acoustic wave propagation. *SIAM J. Sci. Stat. Comput.*, 8(2):135–151, 1987.

[35] B. Strand. Summation by parts for finite difference approximations for d/dx. *J. Comput. Physics*, 110:47–67, 1994.

[36] M. Svärd, J. Gong, and J. Nordström. An accuracy evaluation of unstructured node-centred finite volume methods. *Applied Numerical Mathematics*, 58(8):1142–1158, 2008.

[37] M. Svärd and J. Nordström. On the order of accuracy for difference approximations of initial-boundary value problems. *J. Comput. Physics*, 218:333–352, October 2006.

[38] B. Szilagyl, H.-O. Kreiss, and J.W Winicour. Modeling the black hole excision problem. *Physical Review D*, 71:104035, 2005.

[39] S. V. Tsynkov. Numerical solution of problems on unbounded domains. a review. *Applied Numerical Mathematics*, pages 465–532, 1998.

[40] J. Virieux. Sh-wave propagation in heterogeneous media: Velocity-stress finite-difference method. *Geophysics*, 49:1933–1957, 1984.

[41] J. Virieux. P-sv wave propagation in heterogeneous media: Velocity-stress finite-difference method. *Geophysics*, 51:889–901, 1986.

[42] K.S. Yee. Numerical solution of initial boundary value problems involving maxwells equations in isotropic media. *IEEE Trans. Antennas Propag.*, 14:302–307, 1966.